Molecules and Cells

Crystal Structure of the Pneumococcal Vancomycin-Resistance Response Regulator DNA-Binding Domain

Sang-Sang Park[1], Sangho Lee[2,*], and Dong-Kwon Rhee[1,*]

[1]School of Pharmacy, Sungkyunkwan University, Suwon 16419, Korea, [2]Department of Biological Sciences, Sungkyunkwan University, Suwon 16419, Korea
*Correspondence: sangholee@skku.edu (SL); dkrhee@skku.edu (DKR)
https://doi.org/10.14348/molcells.2021.2235
www.molcells.org

Vancomycin response regulator (VncR) is a pneumococcal response regulator of the VncRS two-component signal transduction system (TCS) of *Streptococcus pneumoniae*. VncRS regulates bacterial autolysis and vancomycin resistance. VncR contains two different functional domains, the N-terminal receiver domain and C-terminal effector domain. Here, we investigated VncR C-terminal DNA binding domain (VncRc) structure using a crystallization approach. Crystallization was performed using the micro-batch method. The crystals diffracted to a 1.964 Å resolution and belonged to space group $P2_12_12_1$. The crystal unit-cell parameters were a = 25.71 Å, b = 52.97 Å, and c = 60.61 Å. The structure of VncRc had a helix-turn-helix motif highly similar to the response regulator PhoB of *Escherichia coli*. In isothermal titration calorimetry and size exclusion chromatography results, VncR formed a complex with VncS, a sensor histidine kinase of pneumococcal TCS. Determination of VncR structure will provide insight into the mechanism by how VncR binds to target genes.

Keywords: crystal structure, response regulator, *Streptococcus pneumoniae*, VncR

INTRODUCTION

Streptococcus pneumoniae (*Spn*) is a human pathogen that causes several serious diseases including pneumonia, otitis media, meningitis, and sepsis. Pneumococcal diseases are treated with antibiotics such as β-lactams and vancomycin. Vancomycin can block bacterial cell wall synthesis, resulting in autolysis of the bacteria. However, *Spn* has demonstrated elevated resistance to vancomycin via VncRS (Novak et al., 1999). VncRS is the one of the two component systems (TCSs) in *Spn*, and is composed of a response regulator (VncR) and a sensor histidine kinase (VncS).

TCSs are the main signaling system for response to environmental changes in most bacteria and plants. When *Spn* encounters new environmental conditions, sensor histidine kinase (HK) is auto-phosphorylated, and subsequently the phosphoryl group of HK is transferred to its cognate response regulator (RR) (Stock et al., 2000). Phosphorylated RRs modulate expression of target genes to adapt to the changing environment. Pneumococcal TCS is classified into four families: Pho, Lyt, Nar, and Agr, while the VncRS system is classified into the Pho family (Paterson et al., 2006). VncR has a helix-turn-helix motif that binds to target DNA and then regulates target gene expression. In *Escherichia coli*, PhoB is important for cell survival in the host and virulence, whereas VncRS is important for vancomycin tolerance in *Spn*. More-

Received 30 November, 2020; revised 10 February, 2021; accepted 25 February, 2021; published online 31 March, 2021

eISSN: 0219-1032

over, pneumococcal autolysis is controlled by VncRS, which senses and responds to cell death signal peptide Pep27 (Haas et al., 2004; Robertson et al., 2002). During autolysis, pneumococcus can release pneumolysin (Ply) toxin (Martner et al., 2008), peptidoglycan particles (Chetty and Kreger, 1981), and lipoteichoic acid (Seo et al., 2008). Ply is a major pneumococcal virulence factor (Martner et al., 2008), and forms oligomeric pore in the host membrane (Tilley et al., 2005). Cell wall particles such as peptidoglycan and lipoteichoic acid stimulate host inflammatory response (Chetty and Kreger, 1981; Seo et al., 2008).

However, the role of pneumococcal VncRS in regulation of pneumococcal virulence is not completely understood. Although VncRS was highly induced in vancomycin-tolerant clinical *Spn* (Sung et al., 2006), the *vncR* mutant strain did not attenuate pneumococcal virulence (Throup et al., 2000), indicating that role of VncRS in pneumococcal virulence is complex. Moreover, deletions of *vncRS* genes did not affect tolerance of vancomycin (Robertson et al., 2002). Previously, we also found that the *vncRS* operon was activated by lactoferrin and that the effector molecule Pep27 was released for pneumococcal lysis. Thus, inactivation of the *pep27* locus renders the mutant lysis and inflammation incompetent, and abrogates lethality even after injection into either the normal mouse brain or the peritoneal cavity of immune-compromised mice (Robertson et al., 2002). Thus, the non-virulent nature of the *pep27* mutant has been utilized for pneumococcal vaccines (Sung et al., 2006). Moreover, interventions involving the VncRS system could facilitate development of novel chemotherapeutics for sepsis and pneumonia treatment. As the first step towards this, we determined the crystal structure of the putative DNA-binding effector domain of VncR, and predicted VncR function. This result will pave the way for development of chemotherapeutics and provide insight into structural and functional role of VncR in *Spn*.

MATERIALS AND METHODS

Protein cloning and purification

Full-length VncR, VncS (194-442) and VncRc (119-242) were amplified by polymerase chain reaction using *S. pneumoniae* D39 (type 2) genomic DNA as a template with each primers (Table 1). Subsequently, the DNA fragments were inserted into the NcoI/XhoI-digested pHis parallel 2 vector (Sheffield et al., 1999). The vectors are transformed into *E. coli* XL1-blue and subsequently transferred to the overexpression strain *E. coli* BL21 (DE3). The recombinant *E. coli* were grown at 37°C to an optical density at 600 nm (OD_{600}) of 0.6 to 0.8 in LB broth with 50 μg/ml ampicillin. VncR, VncRc, and VncS were overexpressed by addition of 1 mM of isopropyl β-D-1-thiogalactopyranoside (IPTG) to the media. Cells were incubated continuously at 25°C for 24 h, and then harvested by centrifugation at 3,382*g* for 10 min. The pellet was resuspended in buffer A (50 mM Tris-HCl pH 7.5, 150 mM NaCl) with 5 mM β-mercaptoethanol and 1 mM phenylmethylsulfonyl fluoride. The suspended pellet was sonicated on ice, and cell debris and insoluble proteins were removed by centrifugation at 16,000*g* for 1 h. Ni-NTA affinity resin

Table 1. List of primers used in this study

Primer	Sequence
pHis-VncS-F (194-)	5'-CGCGGATCCAAGGATGAGATAGGTA-ATCTC-3'
pHis-VncS-R	5'-GGCCCGCTCGAGCTAGTCTTGGAC-GACTTTTGG-3'
pHis-VncR-F	5'-CGCGGATCCATGAAAATTTTAATTG-TAGAAGATG-3'
pHis-VncR-R	5'-GGCCCGCTCGAGCTAGTCTTGGAC-GACTTTTGG-3'
pHis-VncR-F (119-)	5'-CGCGGATCCAAGGATGAGATAGGTA-ATCTCAAG-3'

Restriction enzyme sites incorporated: *BamH1*, GGATCC; *Xho1*, CTCGAG.

Table 2. Data collection and refinement statistics

Parameter	Value
Data collection	
Diffraction source	Beamline 7A, PAL
Wavelength (Å)	0.9795
Temperature (K)	100
Detector	ADSC Quantum 270 CCD
Space group	$P2_12_12_1$
Cell dimensions	
a, *b*, *c* (Å)	25.711, 52.978, 60.615
α, β, γ (°)	90, 90, 90
Mosaicity (°)	0.3
Resolution range (Å)	1.96
Total reflections	6317
Completeness (%)	99.09 (91.22)
Redundancy	13.5
$\langle I/\sigma(I)\rangle$	42.12 (15.86)
$R_{r.i.m.}$	0.079
Overall *B* factor from Wilson plot (Å^2)	27.69
Refinement	
Resolution range (Å)	30.31-1.96 (2.03-1.96)
Completeness (%)	99.09 (91.22)
σ cutoff	0
Final R_{cryst}	0.1717 (0.1874)
Final R_{free}	0.2166 (0.2857)
Protein	818
Ion	-
Ligand	15
Water	66
Total	899
R.M.S.D	
Bonds (Å)	0.006
Angles (°)	0.97
Average *B* factors (Å^2)	
Protein	26.9
Ion	-
Ligand	26.1
Water	32.6
Ramachandran plot	
Favored regions (%)	98
Additionally allowed (%)	-
Outliers (%)	0

(GE Healthcare, UK) was used for purifying VncR with a buffer containing 50 mM Tris-HCl pH 7.5, 500 mM NaCl, and 200 mM Imidazole and for purifying VncRc/VncS (194-442) with a buffer containing 50 mM Tris-HCl pH 7.5, 150 mM NaCl, and 200 mM Imidazole. Tagged-6His was cleaved by TEV-protease during dialysis. Cleaved His-tag, TEV-protease and uncleaved His-tagged protein were removed by using Ni-NTA. Size exclusion chromatography (Superdex S200 or S70 column; GE Healthcare) was performed to remove contaminants. The protein purity was determined using SDS-PAGE and concentrated to 10 mg/ml using a Centricon (Millipore, USA).

Crystallization and structure determination

VncRc crystallization conditions were screened using commercial screening solution kits (Hampton Research, USA) via the microbath method at 22°C. The microbath was covered with a mixture of 50% mineral oil and 50% silicon oil. Crystals were obtained using crystal screen solution (Hampton Research) No. 42 (0.05 M mono-K phosphate, 20% PEG 8K). After crystallization, diffraction data were collected at beamline 7A of Pohang Accelerator Laboratory (Korea) (Jeong et al., 2020). The collected data were merged using HKL2000 software (Otwinowski and Minor, 1997) and the structure was solved by molecular replacement using phaser in the PHENIX program suit (Adams et al., 2011). The final structure models were built in Coot software (Emsley and Cowtan, 2004) and refined by phenix.refine. The refinement information is presented in Table 2. The figure depicting the VncRc structure was rendered with PyMOL.

Full-length VncR and VncS (194-442) interaction assay on analytical size-exclusion chromatography

For full-length VncR and VncS (194-442) interaction assay, full-length VncR and VncS (194-442), which were purified separately, were loaded onto the Superdex S200 column (GE Healthcare) in buffer A with 1 mM DTT, and size-exclusion chromatography was performed using an FPLC system (AKTA FPLC system; GE Healthcare). Subsequently, the major peak fraction containing both VncR and VncS proteins was visualized by Coomassie brilliant blue staining on 15% SDS-PAGE.

ITC experiment

The binding affinity of full-length VncR and VncS (194-442) was calculated using isothermal titration calorimetry (ITC). First, 20 μM full-length VncR in buffer A with 1 mM DTT was placed in the sample cell, and 600 μM VncS (194-442) in the buffer A with 1 mM DTT was injected using a syringe. The total number of injections was 24 in 10-μl volumes. Equilibrium association constants were determined by fitting reference-corrected data using both a one-site and a two-site binding model provided by the manufacturer.

RESULTS AND DISCUSSION

Soluble protein of the C-terminal effector domain of VncR

Most RRs are composed of two domains, the N-terminal receiver domain and the C-terminal effector domain (Fig. 1A). The N-terminal receiver domain structure includes classic α/β folds, whereas the C-terminal effector domain has a helix-turn-helix DNA-binding motif. The N-terminal receiver domain has conserved aspartic acid residue in the middle of the receiver domain, which can receive a phosphate group from the sensor HK. The C-terminal domain can bind to target

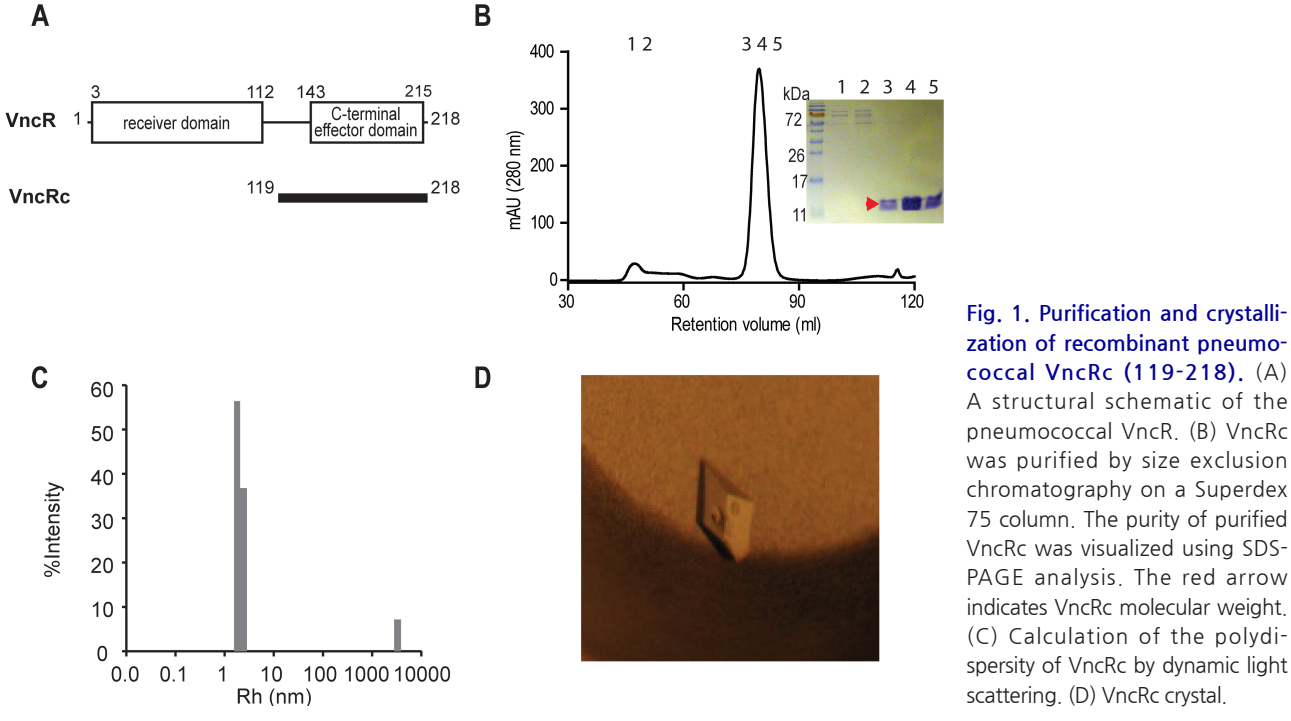

Fig. 1. Purification and crystallization of recombinant pneumococcal VncRc (119-218). (A) A structural schematic of the pneumococcal VncR. (B) VncRc was purified by size exclusion chromatography on a Superdex 75 column. The purity of purified VncRc was visualized using SDS-PAGE analysis. The red arrow indicates VncRc molecular weight. (C) Calculation of the polydispersity of VncRc by dynamic light scattering. (D) VncRc crystal.

DNA and subsequently modulate target gene transcription and translation. The VncRS is a key pneumococcal TCS component responsible for pneumococcal death signal peptide production (Novak et al., 2000). For crystallization, the VncR C-terminal domain (VncRc) was highly purified (Fig. 1B), and the low polydispersity of purified VncRc was confirmed by dynamic light scattering (Fig. 1C). When the VncRc domain was screened using a crystal screening kit, diamond-like crystals were obtained (Fig. 1D). The crystal was diffracted on a Pohang Accelerator Laboratory synchrotron, and the data collected are shown in Table 2.

Overall structure of VncRc (119-242)

First, we compared protein sequence VncR with other PhoB families (Fig. 2A). Generally, receiver domains of RR have more than 2 to 3 conserved Asp, only one of which is as

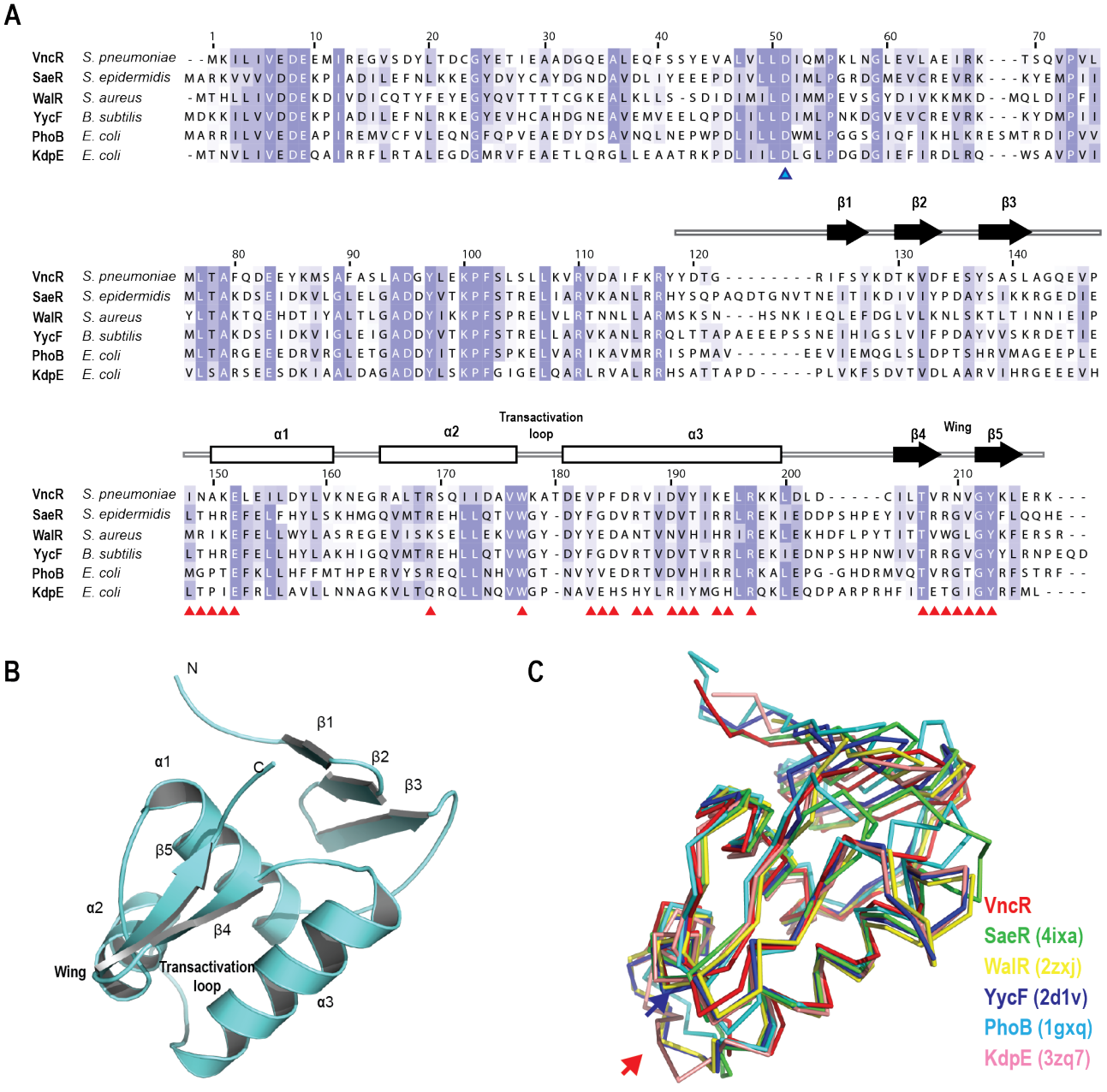

Fig. 2. Sequence alignment and overall structure of VncRc. (A) Comparison of the amino acid sequence of VncR and other Omp-PhoB family members. The amino acid numbering refers to the pneumococcal VncR residue sequence. The secondary structure elements in the VncRc are indicated. The phosphorylation aspartic acid is depicted as a blue triangle. The predicted DNA binding sites are depicted as red triangles. (B) Overall structure of VncRc. (C) Structural superposition of VncRc with other Omp-PhB families. The red and blue arrows indicate the transactivation and wing loop, respectively.

phosphorylation site. Despite RR have conserved functional domains, their sequences are not highly conserved. Therefore, we observed crystal structure of the pneumococcal VncRc. The structure of VncRc is composed of a three-stranded antiparallel β-sheet (β1-β3) on the N-terminal part, followed by a crisscross pattern three-α helical bundle (α1-α3), and a β-hairpin turn (β4-β5) on the C-terminal part (Fig. 2B). Most of RR's have the helix-turn-helix DNA-binding motif on three-α helical bundle (Gao et al., 2007). The helix α3 is important for binding and interacting with target DNA. The transactivation loop, which is important for recognizing target DNA and interacting with sigma factor, is positioned next to the α3 helix (Fig. 2B). The overall structure of VncRc is well superimposed onto structures of DNA-binding domains in OmpR-PhoB superfamily proteins (Fig. 2C) (Blanco et al., 2002).

DNA binding residues in VncRc were predicted using DBD-Hunter software with the structure of the PhoB-DNA complex (Fig. 2A) (Gao and Skolnick, 2008). The orientation of the transactivation loop and wing part of VncRc is slightly different from those of other OmpR-PhoB proteins (Figs. 2B and 2C), which might be related to the distinct mode of interaction between VncR and DNA/RNA polymerase compared to other OmpR-PhoB families.

VncR interacts with its cognate VncS

Generally, RR interacts with its cognate HK for signal transduction. Therefore, we hypothesized that VncR interacts with partner HK, VncS. To check VncR and VncS interaction, we performed size exclusion chromatography with VncR, VncS (194-442) and mixture of VncR and VncS (194-442) (Fig. 3A). The fragment of VncS (194-442) comprises the HAMP (presence of histidine kinases, adenylate cyclases, methyl accepting proteins, and phosphatases), DHp (dimerization and histidine phosphotransfer domain), and CA (catalytic ATP binding domain) domains. The CA acts auto-phosphorylation of histidine residue on DHp by using ATP. Subsequently, auto-phosphorylated VncS binds and transfers the phosphate group to the partner RR. In size exclusion chromatography, a mixture of VncR with VncS (194-442) eluted faster than either VncR or VncS (194-442). Since VncS can form a homo-dimer complex, VncS size should exceed that of monomer VncS (194-442), and size exclusion chromatography results confirmed this. The mixture showed shifted peak indicating a higher molecular weight than either VncS (194-442) or the full-length VncR protein. Moreover, two fractions of the mixture on size exclusion chromatography were observed VncS (194-442) and full-length VncR bands, indicating that VncS (194-442) could interact with its cognate VncR to form a complex (Fig. 3A).

We used unphosphorylated VncS (194-442) with partner full-length VncR for calculating affinity by using ITC. The ITC data showed that the binding K_d of full-length VncR and VncS (194-442) is 49 μM (Fig. 3B). Our results showed that VncS can bind to cognate VncR in the absence of ATP without phosphorylation of VncR or VncS. Thus, VncS can modulate VncR phosphorylation.

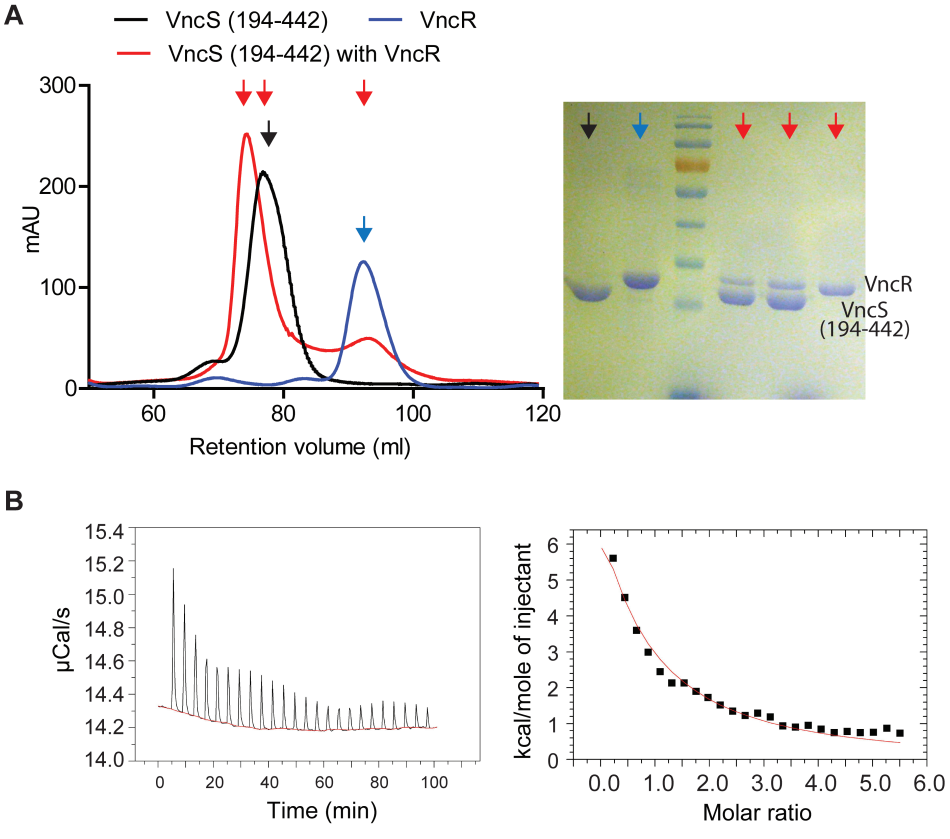

Fig. 3. VncR and VncR complex formation. (A) Black, blue, and red traces represent the eluted solution optical density at 280 nm of VncS (194-442), VncR, and a mixture of VncR and VncS (194-442), respectively, on Superdex S200 chromatography. The main peak fraction of chromatography was loaded on 15% SDS-PAGE and visualized by Coomassie blue staining. The red, blue, and black arrows indicated full-length VncR, VncS (194-442), and a mixture of full-length VncR and VncS (194-442), respectively. (B) Determination of biding affinities of VncR with VncS (191-442) by ITC. The upper panel shows the raw thermogram data; the lower panel shows the heat release after injecting VncS (194-442).

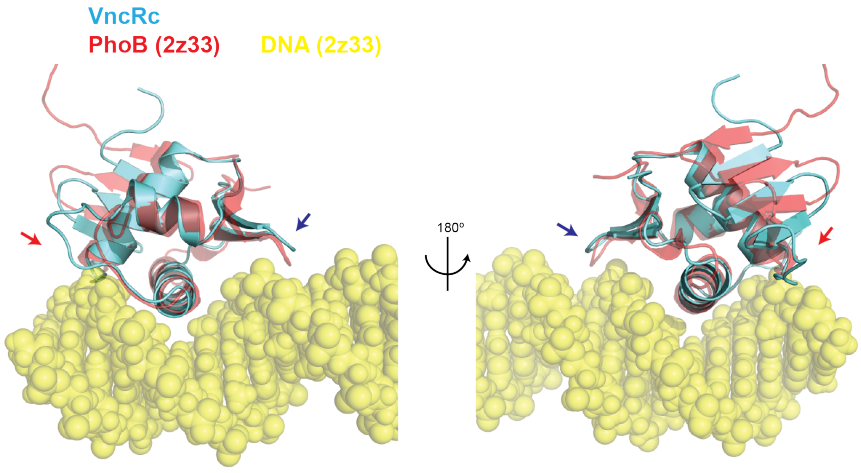

Fig. 4. Model of the VncRc-DNA complex structure. The ribbon structure shows two molecules of VncRc and PhoB. The DNA from the PhoB DNA complex was shown in sphere ace-filling. The color of VncRc and PhoB is cyan and red, respectively. The red and blue arrows indicated the transactivation and wing loop, respectively.

Comparison of VncR with PhoB (OmpR/PhoB) DNA complex structure

To investigate the DNA binding mode of VncR, we superimposed VncR structure with NMR structure of the PhoB DNA complex (Protein Data Bank [PDB] code 2Z33). VncR had low sequence homology with PhoB (24%) but high structure homology with PhoB (a root-mean-square deviation [r.m.s.d.] value of 2.4 using Cα structure only). Moreover, the VncR DNA binding pocket structure is very similar to that of PhoB. Thus, we predicted VncRc-DNA structure interactions by referenced structure of PhoB-DNA interaction (Fig. 4). The VncRc DNA binding residues are Ile148, Asn149, Als150, Lys151, Glu152, Arg169, Trp177, Val183, Pro184, Phe185, Arg187, Val188, Asp190, Val191, Tyr192, Lys194, Glu195, Arg197, Thr207, Val208, Arg209, Asn 210, Val211, Gly212, and Tyr213, respectively (Fig. 2A). When VncRc DNA recognition residues were compared with PhoB DNA recognition residues, Trp177 (PhoB, Trp184) and Arg187 (PhoB, Arg193) were found to be involved in DNA recognition. However, the VncRc DNA recognition residues Val188 (PhoB, Thr194), Tyr192 (PhoB His198), and Lys194 (PhoB, Arg200) are different from those of PhoB. The C-terminal hairpin motif of VncRc also has a very conserved sequence as well as Thr207, Gly213 and Tyr214. However, the orientation of the wing motif in VncRc is different from that of PhoB (Fig. 4). Thus, PhoB and VncR might bind to different target DNA. Recently, we investigated VncR directly binds to pneumococcal capsular polysaccharide locus (Ghosh et al., 2019). Thus, our VncRc structure and DNA binding model will give insights into the transcriptional regulation of CPS biosynthesis-related genes.

ACKNOWLEDGMENTS

This work was supported by the National Research Foundation grants NRF-2018R1A2B6004367 to S.L. and NRF-2018R1A2A1A05078102 to D.K.R. The funding body did not play any role in data collection and analysis, manuscript preparation, or the decision to publish.

AUTHOR CONTRIBUTIONS

S.S.P. conceived and performed experiments and wrote the manuscript. S.L. provided reagents, feedback, and expertise. D.K.R. secured funding and wrote the manuscript.

CONFLICT OF INTEREST

The authors have no potential conflicts of interest to disclose.

ORCID

Sang-Sang Park https://orcid.org/0000-0002-5961-9508
Sangho Lee https://orcid.org/0000-0003-3886-4579
Dong-Kwon Rhee https://orcid.org/0000-0003-2792-3254

REFERENCES

Adams, P.D., Afonine, P.V., Bunkoczi, G., Chen, V.B., Echols, N., Headd, J.J., Hung, L.W., Jain, S., Kapral, G.J., Grosse Kunstleve, R.W., et al. (2011). The Phenix software for automated determination of macromolecular structures. Methods *55*, 94-106.

Blanco, A.G., Sola, M., Gomis-Ruth, F.X., and Coll, M. (2002). Tandem DNA recognition by PhoB, a two-component signal transduction transcriptional activator. Structure *10*, 701-713.

Chetty, C. and Kreger, A. (1981). Role of autolysin in generating the pneumococcal purpura-producing principle. Infect. Immun. *31*, 339-344.

Emsley, P. and Cowtan, K. (2004). Coot: model-building tools for molecular graphics. Acta Crystallogr. D Biol. Crystallogr. *60*, 2126-2132.

Gao, M. and Skolnick, J. (2008). DBD-Hunter: a knowledge-based method for the prediction of DNA-protein interactions. Nucleic Acids Res. *36*, 3978-3992.

Gao, R., Mack, T.R., and Stock, A.M. (2007). Bacterial response regulators: versatile regulatory strategies from common domains. Trends Biochem. Sci. *32*, 225-234.

Ghosh, P., Shah, M., Ravichandran, S., Park, S.S., Iqbal, H., Choi, S., Kim, K.K., and Rhee, D.K. (2019). Pneumococcal VncR strain-specifically regulates capsule polysaccharide synthesis. Front. Microbiol. *10*, 2279.

Haas, W., Sublett, J., Kaushal, D., and Tuomanen, E.I. (2004). Revising the role of the pneumococcal vex-vncRS locus in vancomycin tolerance. J. Bacteriol. *186*, 8463-8471.

Jeong, S., Ahn, J., Kwon, A.R., and Ha, N.C. (2020). Cleavage-dependent activation of ATP-dependent protease HslUV from *Staphylococcus aureus*. Mol. Cells *43*, 694-704.

Martner, A., Dahlgren, C., Paton, J.C., and Wold, A.E. (2008). Pneumolysin released during Streptococcus pneumoniae autolysis is a potent activator

of intracellular oxygen radical production in neutrophils. Infect. Immun. *76*, 4079-4087.

Novak, R., Charpentier, E., Braun, J.S., and Tuomanen, E. (2000). Signal transduction by a death signal peptide: uncovering the mechanism of bacterial killing by penicillin. Mol. Cell *5*, 49-57.

Novak, R., Henriques, B., Charpentier, E., Normark, S., and Tuomanen, E. (1999). Emergence of vancomycin tolerance in Streptococcus pneumoniae. Nature *399*, 590-593.

Otwinowski, Z. and Minor, W. (1997). Processing of X-ray diffraction data collected in oscillation mode. Methods Enzymol. *276*, 307-326.

Paterson, G.K., Blue, C.E., and Mitchell, T.J. (2006). Role of two-component systems in the virulence of Streptococcus pneumoniae. J. Med. Microbiol. *55*, 355-363.

Robertson, G.T., Zhao, J., Desai, B.V., Coleman, W.H., Nicas, T.I., Gilmour, R., Grinius, L., Morrison, D.A., and Winkler, M.E. (2002). Vancomycin tolerance induced by erythromycin but not by loss of vncRS, vex3, or pep27 function in Streptococcus pneumoniae. J. Bacteriol. *184*, 6987-7000.

Seo, H.S., Michalek, S.M., and Nahm, M.H. (2008). Lipoteichoic acid is important in innate immune responses to gram-positive bacteria. Infect. Immun. *76*, 206-213.

Sheffield, P., Garrard, S., and Derewenda, Z. (1999). Overcoming expression and purification problems of RhoGDI using a family of "parallel" expression vectors. Protein Expr. Purif. *15*, 34-39.

Stock, A.M., Robinson, V.L., and Goudreau, P.N. (2000). Two-component signal transduction. Annu. Rev. Biochem. *69*, 183-215.

Sung, H., Shin, H.B., Kim, M.N., Lee, K., Kim, E.C., Song, W., Jeong, S.H., Lee, W.G., Park, Y.J., and Eliopoulos, G.M. (2006). Vancomycin-tolerant Streptococcus pneumoniae in Korea. J. Clin. Microbiol. *44*, 3524-3528.

Throup, J.P., Koretke, K.K., Bryant, A.P., Ingraham, K.A., Chalker, A.F., Ge, Y., Marra, A., Wallis, N.G., Brown, J.R., Holmes, D.J., et al. (2000). A genomic analysis of two-component signal transduction in Streptococcus pneumoniae. Mol. Microbiol. *35*, 566-576.

Tilley, S.J., Orlova, E.V., Gilbert, R.J., Andrew, P.W., and Saibil, H.R. (2005). Structural basis of pore formation by the bacterial toxin pneumolysin. Cell *121*, 247-256.